



1 **Climate engineering and the ocean: effects on biogeochemistry and primary production**

2 Siv K. Lauvset¹, Jerry Tjiputra¹, Helene Muri²,

3 ¹Uni Research Climate, Bjerknes Center for Climate Research, Jahnebakken 5, Bergen,

4 Norway

5 ²University of Oslo, Department of Geosciences, Section for Meteorology and Oceanography,

6 Oslo, Norway

7

8 **ABSTRACT**

9 Here we use an Earth System Model with interactive biogeochemistry to project future ocean
10 biogeochemistry impacts from large-scale deployment of three different radiation
11 management (RM) climate engineering (also known as geoengineering) methods:
12 stratospheric aerosol injection (SAI), marine sky brightening (MSB), and cirrus cloud
13 thinning (CCT). We apply RM such that the change in radiative forcing in the RCP8.5
14 emission scenario is reduced to the change in radiative forcing in the RCP4.5 scenario. The
15 resulting global mean sea surface temperatures in the RM experiments are comparable to
16 those in RCP4.5, but there are regional differences. The forcing from MSB, for example, is
17 applied over the oceans, so the cooling of the ocean is in some regions stronger for this
18 method of RM than for the others. Changes in ocean primary production are much more
19 variable, but SAI and MSB give a global decrease comparable to RCP4.5 (~6% in 2100
20 relative to 1971-2000), while CCT give a much smaller global decrease of ~3%. The spatially
21 inhomogeneous changes in ocean primary production are partly linked to how the different
22 RM methods affect the drivers of primary production (incoming radiation, temperature,
23 availability of nutrients, and phytoplankton) in the model. The results of this work
24 underscores the complexity of climate impacts on primary production, and highlights that



25 changes are driven by an integrated effect of multiple environmental drivers, which all change
26 in different ways. These results stress the uncertain changes to ocean productivity in the
27 future and advocates caution at any deliberate attempt for large-scale perturbation of the Earth
28 system.

29

30 **1 INTRODUCTION**

31 Human emissions of carbon dioxide to the atmosphere is unequivocally causing global
32 warming and climate change (IPCC, 2013). At the 21st United Nations Framework
33 Convention on Climate Change (UNFCCC) Conference of the Parties it was agreed to limit
34 the increase in global mean temperatures to 2°C above pre-industrial levels and to pursue
35 efforts to remain below 1.5°C. Reaching this goal will not be possible without radical social
36 transformation. Solar radiation management (SRM) has been suggested as both a method of
37 offsetting global warming and to reduce risks associated with climate change, substituting
38 some degree of mitigation (Teller et al., 2003, Bickel and Lane, 2009), or to buy time to
39 reduce emissions (Wigley, 2006). Reducing the otherwise large anthropogenic-induced
40 changes in the marine ecosystem drivers (*e.g.*, temperature, oxygen, and primary production)
41 could also be beneficial for vulnerable organisms that need more time to migrate or adapt
42 (Henson et al., 2017). SRM is the idea to increase the amount of solar radiation reflected by
43 Earth in order to offset changes in the radiation budget due to the increased greenhouse effect
44 from anthropogenic emissions, *i.e.* a form of climate engineering – or geoengineering.

45 Here we have performed model experiments with stratospheric sulfur aerosol
46 injections (Crutzen, 2006; Weisenstein et al., 2015), and marine sky brightening (Latham,
47 1990), and cirrus cloud thinning (Mitchell and Finnegan, 2009). Stratospheric aerosol
48 injections (SAI) would involve creating a layer of reflective particles in the stratosphere to
49 reduce the amount of solar radiation reaching the surface. The most widely discussed



50 approach to SAI is to release a gaseous sulfate precursor, like SO₂, which would oxidize to
51 form sulfuric acid and then condensate to reflective aerosol particles. Marine sky brightening
52 (MSB) aims to reflect the incoming solar radiation at lower levels in the atmosphere. Here,
53 the idea is to spray naturally occurring sea salt particles into low-lying stratiform clouds over
54 the tropical oceans to increase the available cloud condensation nuclei, thus increasing the
55 concentration of smaller cloud droplet and increase the reflectivity of the clouds (Latham,
56 1990). The sea salt aerosols are reflective in themselves (*e.g.*, Ma et al., 2008), adding to the
57 cooling potential of the method. Cirrus cloud thinning (CCT) on the other hand, aims to
58 increase the amount of outgoing longwave radiation at the top of the atmosphere. This is
59 envisioned done by depleting the longwave trapping in high ice clouds by seeding them with
60 highly potent ice nuclei (*e.g.*, Mitchell and Finnegan, 2009; Storelvmo et al., 2013). In the
61 absence of naturally occurring ice nuclei, the seeded material would facilitate freezing at
62 lower supersaturations, enabling the growth of fewer and larger ice crystals. These would
63 eventually grow so large that they sediment out of the upper troposphere reducing the lifetime
64 and optical thickness of the cirrus clouds leading to a cooling effect. Together these three
65 methods are referred to as Radiation Management (RM).

66 As pointed out by Irvine et al. (2016) there are several gaps in the research on the
67 impact of RM on both global climate and the global environment considering only a few
68 modelling studies to date systematically compare multiple RM methods. Aswathy et al.
69 (2015) and Niemeier et al. (2013) compared stratospheric sulfur aerosol injections to
70 brightening of marine clouds in terms of the hydrological cycle and extremes in temperatures
71 and precipitation. Crook et al. (2015) compared the three methods used in this study, but
72 restricted the study to temperatures and precipitation. This study focuses on the impact on the
73 ocean carbon cycle, which has several potential climate feedbacks (Friedlingstein et al.,



74 2006), and in particular on ocean primary production, which is known to be temporally and
75 spatially complex.

76 The effect RM has on the ocean carbon cycle and ocean productivity has been studied
77 previously, but limited to the use of simple one-dimensional models (Hardman-Mountford et
78 al., 2013) or with global models but focusing on a single method of RM (Partanen et al.,
79 2016; Tjiputra et al., 2015, Matthews et al., 2009). Due to the many uncertainties and open
80 questions associated with RM impacts, a systematic comparative approach is necessary. The
81 three different methods of RM used in this study are likely to have different effects on both
82 the climate and the ocean due to the differences in the type of forcing being applied. An
83 aspect of RM is that it may allow for continued CO₂ emissions in the future without the
84 accompanied temperature increases and that it does not directly affect the atmospheric CO₂
85 concentrations. Ocean acidification, a direct consequence of increased CO₂ concentrations in
86 the atmosphere, would therefore continue with RM, unless paired with mitigation and carbon
87 dioxide removal.

88 This manuscript is the first to evaluate and compare the effect and impact of multiple
89 RM techniques on ocean biogeochemistry using a fully coupled state-of-the-art Earth system
90 model, and furthermore extends previous studies by looking into impacts introduced by three
91 different large-scale RM deployment scenarios both during and after deployment periods. It is
92 also the first study to assess the impacts of cirrus cloud thinning on ocean biogeochemistry.
93 Our focuses are on impacts on SST, oxygen, pH, and primary production, which are the four
94 climate drivers identified by the Intergovernmental Panel on Climate Change (IPCC),
95 significantly affecting marine ecosystem structure and functioning. In a wider perspective,
96 ocean primary production is often used as an indicator for marine food availability, such as
97 fisheries, so furthering our understanding has direct societal implications and a strong
98 connection to the United Nations Sustainable Development Goals.



99 The model and experiments are described in detail in Section 2, the impacts on ocean
100 temperature, oxygen content, inorganic carbon, and primary production are presented and
101 discussed in Section 3, while Section 4 summarizes and concludes the study.

102

103 **2 METHODS**

104 **2.1 Model description**

105 Three RM methods are simulated using the Norwegian Earth System Model
106 (NorESM1-ME; Bentsen et al., 2013). The NorESM1-ME is a fully coupled climate-carbon
107 cycle model, which has contributed to the fifth assessment of the IPCC and participated in
108 numerous Coupled model intercomparison project phase 5 (CMIP5) analyses. For a full
109 description of the physical and carbon cycle components of the model, the readers are referred
110 to Bentsen et al. (2013) and Tjiputra et al. (2013), respectively. Here, we only briefly describe
111 some key processes in the ocean carbon cycle that are relevant for this study.

112 The ocean carbon cycle component of the NorESM1-ME originates from the Hamburg
113 Oceanic Carbon Cycle Model (HAMOCC; Maier-Reimer et al., 2005). In the upper ocean,
114 the lower trophic ecosystem is simulated using an NPZD-type (Nutrient-Phytoplankton-
115 Zooplankton-Detritus) module. The primary production depends on phytoplankton growth
116 and nutrient availability within the euphotic layer (for some of our calculations assumed to be
117 100 m). In addition to multi-nutrient limitation, the phytoplankton growth is light- and
118 temperature-dependent. The net primary production (NPP) in NorESM1-ME is parameterized
119 using the equations of Six and Maier-Reimer (1996) (Equation 1).

$$120 \quad NPP = r(T, L) * \frac{N}{N+N_o} * P \quad \text{Equation 1}$$

$$121 \quad \text{where } r(T, L) = \frac{f(L)*f(T)}{\sqrt{(f(L)^2+f(T)^2)}} \quad \text{Equation 2}$$



122 N is the concentration of the limiting nutrient (either phosphate, nitrate or dissolved iron), $f(L)$
123 is the function determining light-dependency, $f(T)$ is the function for temperature-dependency,
124 and P is the phytoplankton concentration. Both $f(L)$ and $f(T)$ are defined in Six and Maier-
125 Reimer (1996).

126 In addition to the growth through NPP, the phytoplankton has several sink terms due
127 to mortality, exudation, and zooplankton grazing. All nutrients, plankton, and dissolved
128 biogeochemical tracers are prognostically advected by the ocean circulation. The model
129 adopts a generic bulk phytoplankton and zooplankton compartments. The detritus is divided
130 into organic and inorganic materials: particulate organic carbon, biogenic opal, and
131 calcium carbonate. Organic carbon, once exported out of the euphotic layer, is remineralized
132 at depth – a process that consumes oxygen in the ocean interior. Non-remineralized particles
133 reaching the seafloor undergo chemical reactions with sediment pore water, bioturbation, and
134 vertical advection within the sediment module. The model calculates air-sea CO_2 fluxes as a
135 function of seawater solubility, gas transfer rate, and the gradient of the gas partial pressure
136 (pCO_2) between atmosphere and ocean surface, following Wanninkhof (1992). Prognostic
137 surface ocean pCO_2 is computed using inorganic seawater carbon chemistry formulation
138 following the Ocean Carbon-cycle Model Intercomparison Project (OCMIP).

139 In this study, we make use of ocean primary production calculations made both online
140 by NorESM1-ME and offline, using the monthly averaged output from the model. The offline
141 calculations make use of the same set of equations as the online calculation, but (i) the
142 average value over the top 100 m is used for N , T , and P alike; (ii) L is attenuated to a
143 constant depth of 50 m; (iii) the monthly mean is used for N , T , L , and P . The calculation
144 allows us to decompose and identify the dominant drivers for the simulated changes. The
145 decomposition is done by choosing to keep all but one parameter x constant at a time to
146 quantify the contribution of parameter x to the total change. Table 1 describes how this was



147 done. The parameters being kept constant are kept at the long-term (80 year) monthly mean,
148 as calculated from the pre-industrial model experiment (with constant atmospheric CO₂
149 concentrations).

150

151 **2.2 Experiment setup**

152 SAI, MSB, and CCT were applied individually to the RCP8.5 (Representative
153 Concentration Pathway) future scenario (Table 2). The target of the simulations were to
154 reduce the global mean top of the atmosphere (TOA) radiative flux imbalance of RCP8.5
155 down to RCP4.5. In each experiment, the forcing is applied over years 2020 to 2100. To study
156 the termination effect, the simulations are continued for another 50 years following the
157 cessation of each RM method.

158 Here, the SAI, MSB, and CCT experiments are analyzed and compared to the RCP4.5
159 and RCP8.5 scenarios (Riahi et al., 2011; Thomson et al., 2011) (Table 2). All simulations are
160 run with interactive biogeochemistry and use prescribed anthropogenic CO₂ emissions. The
161 atmospheric CO₂ concentrations are therefore prognostically simulated accounting for land-
162 air and sea-air CO₂ fluxes.

163 The SAI was implemented by prescribing a global layer of sulfate aerosols in the
164 stratosphere, and the optical properties were taken from the ECHAM dataset described in
165 Tilmes et al. (2015). The injection strength was scaled up to 20 TgS in year 2100. The MSB
166 follows the method of Alterskjaer et al. (2013), where the emissions on accumulation mode
167 sea salt was increased over the oceans. Here we choose to apply this to a latitude band of
168 $\pm 45^\circ$. The tropospheric aerosol scheme is fully prognostic, thus allowing the full interactive
169 cycle with clouds and radiation. As for the CCT, we adopt the approach of Muri et al. (2014),
170 where the terminal velocity of ice crystals at typical cirrus forming temperatures of colder
171 than -38°C is increased. The maximum effective radiative forcing was found to be limited at



172 about -3.8 W m^{-2} for CCT, resulting in a somewhat higher top of the atmosphere (TOA)
173 radiative flux imbalance in this simulation at 2100.

174

175 **3 RESULTS AND DISCUSSION**

176 **3.1 Global changes in ocean temperature and oxygen concentration**

177 Relative to the 1971-2000 historical period, the ocean oxygen content in the 200-600
178 m depth interval is projected to decrease by ~6% globally in 2100 in RCP8.5 (Figure 1a). In
179 RCP4.5 on the other hand, the inventory of oxygen in the 200-600 m interval shows only a
180 minor decrease of 2% by 2100 (Figure 1a). This difference stems partly from lower oxygen
181 solubility as the ocean warms and partly from changes in ocean stratification and circulation
182 (not shown). When applying RM to RCP8.5, the oxygen concentration in this depth interval
183 follows the RCP4.5 development closely for all three RM methods (ranging from 2-2.6%
184 decrease in 2100 compared to the 1971-2100 average). There are, however, differences
185 between the methods, with SAI yielding slightly larger decreases after 2060 (Figure 1a). After
186 termination of RM, the rate of oxygen reduction accelerates rapidly for the first ten years,
187 before stabilizing at a new rate of decrease of similar magnitude to that in RCP8.5. The
188 projected oxygen reductions do not drop as low as in RCP8.5 after termination of the RM
189 during our simulation period, but had the simulations been continued for some further
190 decades, the oxygen levels would most likely have converged to the RCP8.5 levels. In 2150,
191 RCP8.5 shows a global mean oxygen decrease globally of 9.5%, while the simulations with
192 terminated RM show a global mean oxygen decrease of 8-8.5% (Figure 1a).

193 In RCP8.5, the global mean sea surface temperatures (SST) are projected to increase
194 by $\sim 2.5 \text{ }^{\circ}\text{C}$ by 2100 relative to 2010 (Figure 1b), and $\sim 3 \text{ }^{\circ}\text{C}$ relative to the 1971-2000 average.
195 With RM, the changes in SST are kept similar to RCP4.5, with an increase ranging from 0.8



196 to 1.1°C over the time period between 2020 (start of RM deployment) and 2100. After
197 termination, there is a very rapid SST increase in the subsequent decade before the SST
198 increases more gradually towards that in RCP8.5. Similar to the development in oxygen
199 content, the absolute change in SST in the model runs with terminated RM is still smaller than
200 the absolute change in RCP8.5 (Figure 1b) in 2150. This is mainly due to the slow response
201 time of the ocean, so the SST would eventually converge had the simulations been carried out
202 for a longer period of time after termination. It should be noted that all methods of RM used
203 in this study have been designed to produce the global mean radiative forcing at the end of the
204 century that is equivalent to the difference in the anthropogenic radiative forcing between
205 RCP4.5 and RCP8.5, *i.e.* 4 W m⁻². This means that the globally averaged sea surface
206 temperature changes, and changes in large-scale physical variables such as oxygen, are
207 expected to be close to those in RCP4.5. The results presented here imply that applying RM
208 does not prevent the long-term impacts of climate change, but would on average delay them.
209 In the case of oxygen concentrations in the 200-600 m depth interval the changes incurred in
210 RCP4.5, as well as when the three different methods of RM are applied, are mostly not
211 significantly different (*i.e.* they are smaller than one standard deviation) from the 1971-2000
212 average (Figure 2). There are a few exceptions where the oxygen changes are significant.
213 These regions, however, highlight how differently the RM methods affect the ocean.

214 The spatial absolute change in SST in 2071-2100 relative to 1971-2000 is shown in
215 Figure 3b for RCP8.5 and Figure 3c for RCP4.5. The changes are significantly smaller in
216 RCP4.5, but the spatial variations are the same in RCP8.5 and RCP4.5. When applying RM,
217 the changes in SST are everywhere smaller than in RCP8.5 at the end of the century. As for
218 thermocline oxygen, the spatial patterns are altered in some regions, as seen in the zonally
219 averaged temperature changes (Figure 3a). The SAI method yields the temperature change
220 most similar to that in RCP4.5, which is also mirrored in the near surface air temperatures



221 (Muri et al., in prep). MSB yields the SST changes that are most different compared to
222 RCP4.5. For this method there is a strong bimodal pattern in the SST changes in the North
223 Pacific (Figure 3e), which is also seen in oxygen (Figure 2e). The tropical and subtropical
224 changes in SST with MSB are linked to an enhancement of the Pacific Walker cell, which is
225 induced when MSB is applied (Alterskjær et al., 2013; Ahlm et al, 2017).

226 Regardless of the RM method, some regions, in particular the northwestern Pacific,
227 will still experience levels of warming (cooling) and oxygen loss (gain) exceeding those in
228 RCP4.5. With SAI, the North American west coast, an important region for aquaculture, will,
229 for example, experience enhanced deoxygenation, which is not projected to happen in
230 RCP4.5. The large spatial heterogeneity in how RM affects ocean temperatures and oxygen
231 concentrations highlights that RM can possibly lead to new and detrimental conditions
232 regionally even if beneficial in the global mean.

233

234 **3.2 Global changes in the inorganic ocean carbon cycle**

235 The atmospheric CO₂ concentration continue to rise in all experiments in which RM is
236 applied at the same rate as in RCP8.5 (Figure 4a), given no simultaneous mitigation efforts in
237 these cases. The atmospheric CO₂ concentration in 2100 in RCP8.5 is 1109 ppm and in 2150
238 it is 1651 ppm. In 2100 there is a minor reduction in CO₂ concentrations when RM is applied
239 of 13 -21 ppm compared to RCP8.5, depending on method. MSB gives the largest decrease in
240 atmospheric CO₂. The termination of RM does not significantly affect the atmospheric CO₂
241 evolution and in 2150 there is a marginal reduction of -15 to -26 ppm depending on method,
242 again with MSB giving the largest reduction. The reductions in atmospheric CO₂
243 concentrations when applying RM are due to the decreasing ocean temperatures leading to
244 larger air-sea flux of CO₂ (Figure 4b). Note that the land carbon sinks also increase slightly



245 when RM is applied (Tjiputra et al., 2016). The lower CO₂ concentration with MSB is due to
246 the forcing from MSB being applied over the oceans, and the cooling of the ocean in many
247 regions thus being stronger for this method of RM (Figure 3).

248 While RM leads to a small increase global mean oceanic CO₂ uptake from the
249 atmosphere, due to increased solubility, the difference introduced by each method is not
250 outside of the interannual variability of RCP8.5 up to 2075. By 2100, the different RM
251 methods give an additional CO₂ uptake of ~0.5 PgC yr⁻¹. After termination, the uptake
252 anomaly quickly drops and returns to the same level as RCP8.5 within only two years. Future
253 surface ocean pH is forced by the increasing atmospheric CO₂ concentrations, which drive the
254 uptake of CO₂ in the surface ocean. Thus RM could possibly worsen future ocean
255 acidification, unless atmospheric CO₂ concentrations are dealt with. However, given the small
256 changes in both atmospheric concentrations and ocean uptake stemming from RM, the surface
257 pH is not greatly affected by RM (Figure 4c). Hence, termination does not considerably affect
258 the pH decrease on the surface ocean.

259 Anthropogenic changes in the ocean inorganic carbon content comes from the top
260 down, so it takes a long time for these changes to be observable in the deep ocean. Therefore,
261 the globally averaged deep ocean (>2000 m) pH changes by only 0.06 pH units between 2010
262 and 2150 in RCP8.5 (Figure 4d). The only region where pH changes significantly in the deep
263 ocean is the North Atlantic north of 30°N, where the strong overturning circulation brings
264 anthropogenic carbon to great depths in a relatively short timeframe. Here there is a
265 significant decrease in deep ocean pH between 2010 and 2150 in RCP8.5, as well as the three
266 RM cases (Figure 4e). In RCP8.5, the pH is projected to decrease by ~0.2 pH unit in 2100.
267 RM leads to an additional acidification of 0.02-0.045 (depending on the method of RM) in the
268 deep North Atlantic Ocean, which is large enough to marginally, but not significantly, affect
269 the global average (Figure 4d). A similar result was found by Tjiputra et al. (2015). After



270 termination of RM, the pH keeps decreasing – now at a rate comparable to RCP8.5. This
271 change in rate of decrease after termination happens within ~10 years, indicating that the
272 changes in the inorganic carbon cycle are very quick in the North Atlantic. Both the rapid
273 decrease of deep ocean pH in this region and the rapid recovery towards RCP8.5 development
274 after termination of RM, are likely linked to changes in the Atlantic Meridional Overturning
275 Circulation due to climate change and RM (not shown, see Muri et al., in prep.). While the
276 global mean pH below 2000m in RM experiments rebound to that of the RCP8.5, this is not
277 the case for the North Atlantic. In the latter, all RM methods lead to and remain at lower pH
278 than the RCP8.5 by 2150. It is likely that the deep pH in the North Atlantic would recover to
279 that in RCP8.5 had the simulations been continued for another few decades, but we have no
280 way of analyzing how long that would take.

281

282 3.3 Global changes in ocean primary production

283 The direct effects of RM on surface shortwave radiation and temperature directly
284 affect photosynthesis through the light and temperature dependence of the phytoplankton
285 growth rate. The ocean productivity, and by extension ocean biological carbon pump, is thus
286 indirectly affected by RM. There is a lot of interannual variability in the primary production
287 changes hence Figure 5 shows the 5-year running averages of relative changes to the 1971-
288 2000 average. In RCP8.5, there is a decrease of ~10% by 2100 (Figure 5), which is within the
289 range of the decrease projected by CMIP5 models of $-8.6 \pm 7.9\%$ (Bopp et al., 2013) and
290 mainly due to the overall warming leading to a more stratified ocean where there are less
291 nutrients available in the euphotic zone. All RM methods also exhibit decreases in ocean
292 primary productivity, but these are all smaller than those in RCP8.5. The shortwave-based
293 methods, *i.e.*, SAI and MSB, which reduce the amount of downward solar radiation at the
294 surface, have the largest decreases (~6% in 2100) of the RM methods, which is more of a



295 decrease than in RCP4.5. The longwave-based CCT method, however, yields only a minor
296 decrease of ~3% in 2100, *i.e.* less than in RCP4.5. As the cirrus clouds are thinned or
297 removed, more sunlight reaches the surface ocean, thus promoting and increasing primary
298 above the RCP4.5 levels. The divergence between methods is particularly strong in the period
299 2070-2100, as the radiative forcing by RM approaches -4 Wm^{-2} . After termination, it takes
300 less than five years for the development of ocean primary production to return to RCP8.5
301 levels again.

302 On average there are some interesting spatial features in how primary production
303 changes. Figure 6a shows the zonally averaged difference between 2071-2100 and 1971-
304 2000. In the Northern Hemisphere, primary production decreases everywhere, and decreases
305 less in RCP4.5 and with RM than in RCP8.5. In the Southern Hemisphere, on the other hand,
306 the changes in primary production are much more spatially variable, and the response to the
307 different methods of RM is more variable. Between the Equator and 40°S there is a reduction
308 in primary production in 2071-2100 relative to 1971-2000, while south of 40° there is
309 generally an increase (except in a narrow band at 60°S). In the Southern Hemisphere the
310 impact of CCT is quite different from the impact of SAI and MSB. This is probably due to the
311 change in radiative balance, which is much stronger for CCT in the southern high latitudes
312 than for the other methods (not shown, see Muri et al., in prep.). Because of the large spatial
313 and inter-annual variability, the changes incurred to ocean primary production in the future
314 are frequently not significantly different (*i.e.* the absolute change is smaller than one standard
315 deviation) from the 1971-2000 average (Figure 6b-f). This means that when RM is applied,
316 the ocean primary production does not change in most of the ocean. However, it is clear that
317 the changes in primary production in 2071-2100 relative to 1971-2000 are smaller in RCP4.5
318 than in RCP8.5 (Figures 6b and 6c), and that the spatial variations in all experiments mainly
319 come from the nutrient availability (not shown), which is furthermore dependent on ocean



320 stratification. There are also some regions of significant change in ocean primary production,
321 which are discussed further in Section 3.5.

322

323 **3.4 Drivers of global changes in ocean primary production**

324 To further evaluate how RM affects ocean primary production, we have made offline
325 calculations using Equation 1 and the monthly mean model output of nitrate, phosphate, iron,
326 and phytoplankton concentration, temperature, and shortwave radiation input at the surface, as
327 described in Section 2. For the top 100 m of the ocean, only CCT significantly changes
328 primary production compared to RCP8.5. In fact, CCT results in an increased productivity by
329 2100 (Figure 7a), which is linked to the increase in the incoming shortwave solar radiation in
330 some regions, since the shortwave reflection from ice clouds is reduced. After termination of
331 CCT, the primary production drops to the same level as RCP8.5 within two years. The
332 RCP4.5 scenario yields little change by 2100. The fact that CCT shows a significant global
333 increase in ocean primary production relative to RCP8.5 and even a positive change at the end
334 of the century is a very interesting result of this study. It suggests that when considering the
335 global ocean primary production changes alone, implementation of CCT may offer the least
336 negative impact of the three tested methods. The side effect, however, is that once terminated,
337 CCT method could lead to most drastic change in primary production over very short period.

338 Warmer temperatures increase growth rates. Thus primary production increases when
339 only temperature is allowed to change in the offline calculation, as temperature increases in
340 all scenarios considered here (Figure 7b). All methods of RM yield an increase in primary
341 production of ~1% from 2020 to 2100, comparable to RCP4.5, in this calculation. This is
342 consistent with SST being comparable between RCP4.5 and RM (Figure 1b). After
343 termination, the temperature-induced primary production increases rapidly for the first five



344 years before stabilizing with the same rate of change as that in RCP8.5. Just like SST (Figure
345 1b), the absolute change in primary production does not recover to the quite the same absolute
346 level as that in RCP8.5, but all simulations show an increase in primary production of ~3% by
347 2150.

348 Reduced shortwave radiation at the surface lead to decreased primary production. In
349 RCP4.5 and RCP8.5, light constraints do not change much, hence the primary production also
350 does not considerably change when only shortwave radiation is allowed to vary in the offline
351 calculation (Figure 7c). Both SAI and MSB decrease the amount of global mean direct
352 shortwave radiation at the surface, however, which negatively affect the phytoplankton
353 growth rate and primary production in the ocean (Figure 7c). The result of allowing only
354 shortwave radiation to vary is therefore a decrease in primary production of ~2% by 2100 for
355 SAI and MSB (Figure 7c). When reducing the optical thickness and the lifetime of the cirrus
356 clouds in the model, the shortwave reflection by these clouds is reduced, allowing more
357 shortwave radiation to reach the surface. CCT thus results in an increase in primary
358 production of ~2% by 2100 (Figure 7c). It is this increase in available shortwave radiation
359 that causes the majority of the increase in ocean productivity with CCT, with some
360 contribution from the elevated temperatures (Figure 7b). Within two years of the termination
361 of RM, the simulated primary production has completely returned to the baseline conditions.

362 Inorganic nutrients are also important limiting factors, especially in the low latitude
363 regions. Given the formulation of Equation 1, we use phytoplankton concentration as a proxy
364 for nutrient availability when calculating primary production. Note though, that the
365 relationship between nutrients and phytoplankton is not exactly one to one because
366 phytoplankton are also grazed by zooplankton in the model. However, temporal changes in
367 phytoplankton concentration give a strong indication of how the stratification limits access to
368 nutrients in the surface ocean. Figure 7d shows that phytoplankton is the dominant factor



369 determining changes in ocean primary production, except when CCT is applied. When only
370 phytoplankton concentration is allowed to vary temporally in the offline calculation there is a
371 decrease of ~8% by 2100 in RCP8.5. The SAI and MSB methods of RM also exhibit a change
372 in primary production, but the change of ~5% is less than that in RCP8.5. With CCT there is
373 no significant change in primary production by 2100. After termination, the phytoplankton-
374 driven change of ocean productivity decreases rapidly and after 4-5 years it continues
375 changing at a rate comparable to that in RCP8.5, reaching a global mean reduction of greater
376 than -10% in 2150.

377

378 **3.5 Regional changes in ocean primary production**

379 As seen in Figure 6, the projected changes in ocean primary production exhibit large
380 spatial variation. Applying RM does not change the large-scale spatial heterogeneity, but
381 rather works to enhance or weaken the change magnitude (Figure 6). These regional
382 differences are important since regional changes are much more important than global
383 changes when determining the impact changes in ocean primary production has on human
384 food security (Mora et al., 2013). For a more detailed analysis, five regions have been
385 identified and analyzed. These regions are chosen based on:

- 386 (i) a significant change in primary production in RCP8.5 in years 2071-2100 relative to
387 1971-2000;
- 388 (ii) the sign of the change in ocean primary production projected by NorESM1-ME being
389 consistent with that of the CMIP5 models ensemble (Bopp et al., 2013; Mora et al.,
390 2013);
- 391 (iii) the impact the different methods of RM has on this increase or decrease in the online
392 simulations; and



393 (iv) their relative importance for fish catches, as identified in Zeller et al. (2016).

394 The regions are outlined in black in Figure 6b, and labeled the Equatorial Pacific,
395 Equatorial Atlantic, Southern Atlantic, Indian Ocean, and Sea of Okhotsk in Figure 8. In
396 RCP8.5, the Sea of Okhotsk and Southern Atlantic exhibit a significant increase in primary
397 production in 2071-2100 relatively to 1971-2000, while the Equatorial Pacific, Indian Ocean,
398 and Equatorial Atlantic show a significant weakening (Figure 8). Given the lack of
399 complexity and lack of higher trophic level organisms in the NorESM1-ME, we are unable to
400 directly link changes in primary production to impacts on the higher trophic levels in this
401 study. But given the changes in Arctic biodiversity observed today due to temperature
402 changes (*e.g.* Bucholz et al., 2012; Fossheim et al., 2015), respective changes in migration
403 pattern would be likely to happen with RM. It cannot be assumed from our results that
404 increased primary production will lead to increased fish stocks and thus potential for higher
405 fish catches, because the driving factors leading to higher primary production (*i.e.*
406 temperature, light availability, and stratification) could also lead to biodiversity changes.
407 Higher primary production does lead to more food for higher trophic level organisms,
408 therefore a significant decrease in regional primary production is likely to decrease higher
409 trophic organisms due to less food availability in those regions. Based on the model
410 projections, it is possible that there will be less fish catches in the Indian Ocean and
411 Equatorial Atlantic in the future than today. The different methods of RM also lead to
412 different effects on ocean primary production (Figure 6 and 8), and in the Equatorial Atlantic
413 and in the shaded regions where there is no significant changes, do all three methods give
414 changes in primary production comparable to those in RCP4.5.

415 In the Equatorial Pacific RCP8.5 leads to a decrease in ocean primary production of
416 21% in 2071-2100 relative to 1971-2000, driven by changes in phytoplankton concentration
417 (our proxy for circulation changes). Changes in circulation dominates the change of 12%



418 incurred in RCP4.5 too. This region is today a very productive fishery area (Zeller et al.,
419 2016), so a significant decrease in primary production could have adverse effects on fish
420 catches. It is therefore noteworthy that all RM methods yield primary production changes
421 only marginally smaller than those in RCP8.5, and not nearly as small as those in RCP4.5.
422 Radiation changes become more important in driving changes with RM, which is consistent
423 with changes in cloud fraction (not shown, see Muri et al., in prep.). With CCT the radiation
424 changes yield an increase in primary production of 5% indicating that this is one of the
425 regions that drive the global mean increase in primary production with CCT (Figure 7a). After
426 termination, the change in primary production is comparable to that in RCP8.5 in all
427 experiments, and the warming incur a small increase in primary production of ~2%.

428 The Southern Atlantic has the largest changes in 2071-2100 relative to 1971-2000
429 where RCP8.5 results in an increase in ocean primary production of 39% and RCP4.5 leads to
430 an increase of 25%. SAI leads to changes in primary production comparable to that in
431 RCP8.5, while MSB and CCT yielding changes more in line with RCP4.5. For all
432 experiments changes in phytoplankton concentration is the dominant factor indicating that
433 changes in circulation will be substantial here. Changes in temperature contribute ~5% to the
434 total change which is consistent with a significant warming in all experiments (Figure 3). This
435 alleviates the temperature limitation of phytoplankton growth, which is consistent with the
436 other CMIP5 models (Bopp et al., 2013). After termination, the increase continues in the
437 Southern Atlantic, and in 2121-2150 the changes in primary production are 50-60% higher
438 than in 1971-2000 in all experiments.

439 In the Sea of Okhotsk changes in temperature yield changes in primary production
440 comparable with that in RCP4.5 (13%), which is marginally smaller than that in RCP8.5
441 (18%). SAI and MSB both yield changes comparable to that in RCP4.5, while CCT, on the
442 other hand, is comparable to RCP8.5. In all experiments, temperature changes are an



443 important driver of the overall increases in primary production, which is consistent with the
444 strong warming in this region (Figure 3). After termination, all experiments yield comparable
445 increases in primary production, and the temperature changes have the largest contribution to
446 the overall increase, which is consistent with strong warming when RM is terminated.

447 In the Equatorial Atlantic there is a reduction of ocean primary production in RCP8.5
448 of 19% in 2071-2100 relative to 1971-2000. Changes in phytoplankton concentration
449 dominate this change, with a minor contribution of <5% from radiation changes. All methods
450 of RM yield changes in ocean primary production more in line with that in RCP4.5 (11%), but
451 changes in radiation are more important with SAI and MSB. After termination, all
452 experiments result in the same decrease in ocean primary production of 25%.

453 In the Indian Ocean there is also a reduction of ocean primary production in RCP8.5.
454 Here the total change in 2071-2100 is 21%, but unlike in any other regions the temperature
455 induced changes lead to only a small increase of 1-2% in all experiments. This is consistent
456 with parts of this region experiencing a small decrease in SST (Figure 3). Both SAI and MSB
457 yield changes in primary production comparable to that in RCP8.5 (19% and 18%
458 respectively), but where changes in radiation contribute ~2% to the total reduction. There is,
459 however, no corresponding change in cloud cover (see Muri et al., in prep.) to explain the
460 apparent importance of radiation changes in this region. The Indian Ocean is also one of the
461 regions where CCT able to sustain (i.e., induce least changes) the contemporary primary
462 production. After termination, the ocean primary production continues to decrease and is in
463 2121-2150 30% lower than in 1971-2000 in all experiments. Unusually, the temperature
464 changes lead to an increase in ocean primary production of 4% in 2121-2150 in all
465 experiments.

466



467 **3.6 Comparison with previous studies**

468 Very few other studies have been published on the impact on ocean biogeochemistry
469 due to RM, but two recent ones are Tjiputra et al. (2016) and Partanen et al. (2016). Tjiputra
470 et al. (2016) identified changes in ocean primary production and export production in a
471 simulation with SAI. The implementation of SAI is different here both in methodology and
472 amplitude of forcing, but the spatial signal of surface climate response and the overall impact
473 on global ocean primary production is broadly comparable. Nevertheless, our study provides
474 a more extended analysis in identifying the dominant drivers of changes in primary
475 production in key ocean regions. Partanen et al. (2016), on the other hand, analyzed the
476 effects on ocean primary production from MSB only. Overall, the effects of MSB in this
477 study and that of Partanen et al. (2016) are quite different both spatially and as a function of
478 time. This is likely due to the several noteworthy differences between their method and the
479 one used here:

- 480 (i) Partanen et al. (2016) uses the UVic ESCM model, an Earth system model of
481 intermediate complexity (EMIC) while here we use the fully coupled NorESM1-ME
482 Earth system model;
- 483 (ii) the RM forcing applied by Partanen et al. (2016) is -1 Wm^{-2} annually, while here it is
484 scaled up to -4 Wm^{-2} in 2100;
- 485 (iii) Partanen et al. (2016) applies RM to RCP4.5 while here we apply RM to RCP8.5;
- 486 (iv) Partanen et al. (2016) applies RM for 20 years before termination while here we
487 apply RM for 80 year before termination, which, combined with the higher forcing,
488 means that the Earth system takes longer to recover in this study than in the Partanen
489 et al. (2016) study.

490 The biggest and most important of these differences is that Partanen et al. (2016) use
491 an EMIC while we use an ESM. The ecosystem module in NorESM1-ME is not substantially



492 more complex than that of the UViC ESCM model, but differences could arise due to better
493 representation of the ocean physical circulation (owing to higher spatial resolution) and air-
494 sea interactions. Differences in the aerosol-cloud-climate interactions will also affect the
495 results. NorESM1-ME has a fully interactive tropospheric aerosol scheme, which is of key
496 importance when evaluating the impact of changes in shortwave radiation reaching the
497 surface from changes to clouds. Partanen et al. (2016) identify a decrease in global mean
498 ocean primary production relative to their reference case (RCP4.5) while in our MSB
499 simulation we simulate an increase in ocean primary production relative to our reference case
500 (RCP8.5). These differences and the large differences in the spatial impact can partly be
501 explained by the differences in the applied RM forcing and method, but is mostly explained
502 by the fundamental differences between the models and especially how clouds are modelled.
503 Another important difference between Partanen et al. (2016) and this study is the timing of
504 termination, since this is a very important aspect of all climate engineering studies. Partanen
505 et al. (2016) applies RM for 20 years before termination, while we apply RM for 80 years
506 before termination. This means that in our study the impact on temperature and ocean
507 circulation is greater than in the Partanen et al. (2016) study as the slow climate feedbacks are
508 allowed to pan out. This could explain the differences in termination effect between the
509 studies, where the primary production fully recovers and exceeds that in RCP4.5 in the
510 Partanen et al. (2016) study, but remain within the variability of RCP8.5 here. The larger
511 magnitude of the forcing applied in our simulations (-4 Wm^{-2} in 2100) also means that it takes
512 much longer for the climate system to recover back to the RCP8.5 state.

513

514 4 CONCLUSIONS

515 In this study, we use the Norwegian Earth System Model with fully interactive carbon
516 cycle to assess the impact of three radiation management climate engineering (RM) methods



517 on marine biogeochemistry. The model simulations indicate that RM may reduce
518 perturbations in SST and thermocline oxygen driven by anthropogenic climate change, but
519 that large changes in primary production remain and are even intensified in some regions. It
520 must be noted that we use only one model, and that such models are known to have large
521 spread in their projections of future ocean primary production (*e.g.* Bopp et al., 2013).
522 However, this single-model study does show some clear tendencies:

- 523 (i) A clear mitigation of the global mean decrease in ocean primary production from
524 10% in 2100 in RCP8.5 and ~5% in RCP4.5 to somewhere between 3% and 6%
525 depending on the method of RM.
- 526 (ii) Strong regional variations in the changes, and what primarily drives the changes, in
527 ocean primary production. The different methods of RM do not have the same effects
528 in the same regions, even though SAI and MSB yield similar global averages.
- 529 (iii) MSB yields the largest changes relative to RCP4.5, which is consistent with MSB
530 being applied over the ocean and therefore likely affects the ocean more strongly than
531 the other methods.

532 The effect of future climate change on ocean primary production is uncertain, and is
533 driven by an integrated change in physical factors such as temperature, radiation, and ocean
534 mixing. Additionally, changes in ocean oxygen concentrations and ocean acidification are
535 likely to affect ocean primary production. So it is noteworthy that with RM, anthropogenic
536 CO₂ emissions are not curbed, so ocean acidification would continue. The results presented in
537 this study show that future changes to ocean primary production would likely be negative on
538 average, but exhibit great variation both temporally and spatially, regardless of whether or not
539 RM is applied.



540 This study also show that for the first five to ten years after a sudden termination of
541 large-scale RM the SST, oxygen, surface pH, and primary production all experience changes
542 that are significantly larger than those projected without RM implementation or mitigation.
543 While there is still large uncertainty in how marine habitats respond to such rapid changes, it
544 is certain than they will have less time to adapt or migrate to a more suitable location and
545 potentially have higher likelihood to face extinction.

546 The results of this work does nothing to diminish the complexity of climate impacts on
547 primary production, but rather highlights that any change in ocean primary production is
548 driven by a combination of several variables which all change in different ways in the future,
549 and subsequently are affected differently when RM is applied. The importance of ocean
550 primary production for human societies, however, lies in its impact on food security in
551 general and fisheries in particular, for which regional changes are much more important than
552 global changes (Mora et al., 2013).

553

554 **ACKNOWLEDGEMENTS**

555 The authors acknowledge funding from the Norwegian Research Council through the project
556 EXPECT (229760). We also acknowledge NOTUR resource NN9182K, Norstore NS9033K
557 and NS1002K. Helene Muri was also supported by RCN project 261862/E10, 1.5C-BECCSy.
558 JT also acknowledges RCN project ORGANIC (239965). The authors want to thank Alf Grini
559 for his technical assistance in setting up and running model experiments and as well as the
560 rest of the EXPECT team

561

562 **REFERENCES**

- 563 Ahlm, L., Jones, A., Stjern, C. W., Muri, H., Kravitz, B., and Kristjánsson, J. E.: Marine
564 cloud brightening – as effective without clouds, *Atmos. Chem. Phys. Discuss.*, 2017,
565 1-25, 2017. doi:10.5194/acp-2017-484.
- 566 Alterskjær, K., Kristjánsson, J. E., Boucher, O., Muri, H., Niemeier, U., Schmidt, H., Schulz,
567 M., and Timmreck, C.: Sea-salt injections into the low-latitude marine boundary layer:
568 The transient response in three Earth system models, *J. Geophys. Res.-Atmos.*, 118,
569 12195-12206, 2013. doi:10.1002/2013jd020432
- 570 Aswathy, N., Boucher, O., Quaas, M., Niemeier, U., Muri, H., Mulmenstadt, J., and Quaas, J.:
571 Climate extremes in multi-model simulations of stratospheric aerosol and marine
572 cloud brightening climate engineering, *Atmospheric Chemistry and Physics*, 15, 9593-
573 9610, 2015. doi:10.5194/acp-15-9593-2015
- 574 Bentsen, M., Bethke, I., Debernard, J. B., Iversen, T., Kirkevåg, A., Seland, Ø., Drange, H.,
575 Roelandt, C., Seierstad, I. A., Hoose, C., and Kristjánsson, J. E.: The Norwegian Earth
576 System Model, NorESM1-M – Part 1: Description and basic evaluation of the physical
577 climate, *Geosci. Model Dev.*, 6, 687-720, 2013. doi:10.5194/gmd-6-687-2013
- 578 Bickel J, and Lane L. *An Analysis of Climate Engineering as a Response to Climate Change.*
579 Frederiksberg: Copenhagen Consensus Center. 2009.
- 580 Bopp, L., Resplandy, L., Orr, J. C., Doney, S. C., Dunne, J. P., Gehlen, M., Halloran, P.,
581 Heinze, C., Ilyina, T., Seferian, R., Tjiputra, J., and Vichi, M.: Multiple stressors of
582 ocean ecosystems in the 21st century: projections with CMIP5 models,
583 *Biogeosciences*, 10, 6225-6245, 2013. doi:10.5194/bg-10-6225-2013
- 584 Buchholz, F., Werner, T., and Buchholz, C.: First observation of krill spawning in the high
585 Arctic Kongsfjorden, west Spitsbergen, *Polar Biology*, 35, 1273-1279, 2012.
586 doi:10.1007/s00300-012-1186-3
- 587 Crook, J. A., Jackson, L. S., Osprey, S. M., and Forster, P. M.: A comparison of temperature
588 and precipitation responses to different Earth radiation management geoengineering
589 schemes, *J. Geophys. Res.-Atmos.*, 120, 9352-9373, 2015. doi:10.1002/2015jd023269
- 590 Crutzen, P. J.: Albedo enhancement by stratospheric sulfur injections: A contribution to
591 resolve a policy dilemma? *Climatic Change*, 77, 211-219, 2006. doi:10.1007/s10584-
592 006-9101-y
- 593 Fossheim, M., Primicerio, R., Johannesen, E., Ingvaldsen, R. B., Aschan, M. M., and Dolgov,
594 A. V.: Recent warming leads to a rapid borealization of fish communities in the
595 Arctic, *Nat. Clim. Chang.*, 5, 673-677, 2015. doi:10.1038/nclimate2647
- 596 Friedlingstein, P., Cox, P., Betts, R., Bopp, L., von Bloh, W., Brovkin, V., Cadule, P., Doney,
597 S., Eby, M., Fung, I., Bala, G., John, J., Jones, C., Joos, F., Kato, T., Kawamiya, M.,
598 Knorr, W., Kindsay, K., Matthews, H. D., Raddatz, T., Rayner, P., Reick, C.,
599 Roeckner, E., Schnitzler, K.-G., Schnur, R., Strassmann, K., Weaver, A. J.,
600 Yoshikawa, C., and Zeng, N.: Climate-Carbon Cycle Feedback Analysis: Results from
601 the C4MIP Model Intercomparison, *Journal of Climate*, 19, 3337-3353, 2006.
- 602 Henson, S. A., Beaulieu, C., Ilyina, T., John, J. G., Long, M., Séférian, R., Tjiputra, J., and
603 Sarmiento, J. L.: Rapid emergence of climate change in environmental drivers of
604 marine ecosystems, *Nat. Commun.*, 8, 14682, 2017. doi:10.1038/ncomms14682



- 605 Hardman-Mountford, N. J., Polimene, L., Hirata, T., Brewin, R. J. W., and Aiken, J.: Impacts
606 of light shading and nutrient enrichment geo-engineering approaches on the
607 productivity of a stratified, oligotrophic ocean ecosystem, *J. R. Soc. Interface*, 10, 9,
608 2013. doi:10.1098/rsif.2013.0701
- 609 IPCC, 2013: Climate Change 2013: The Physical Science Basis. Contribution of Working
610 Group I to the Fifth Assessment Report of the Intergovernmental Panel on Climate
611 Change [Stocker, T.F., D. Qin, G.-K. Plattner, M. Tignor, S.K. Allen, J. Boschung, A.
612 Nauels, Y. Xia, V. Bex and P.M. Midgley (eds.)]. Cambridge University Press,
613 Cambridge, United Kingdom and New York, NY, USA, 1535 pp.
- 614 Irvine, P. J., Kravitz, B., Lawrence, M. G., Gerten, D., Caminade, C., Gosling, S. N., Hendy,
615 E., Kassie, B., Kissling, W. D., Muri, H., Oeschle, A., and Smith, S. J.: Towards a
616 comprehensive climate impacts assessment of solar geoengineering, *Earth's Future*,
617 2016. doi:10.1002/2016EF000389
- 618 Kristjansson, J. E., Muri, H., and Schmidt, H.: The hydrological cycle response to cirrus cloud
619 thinning, *Geophysical Research Letters*, 42, 10807-10815, 2015.
620 doi:10.1002/2015gl066795
- 621 Latham, J.: Control of Global Warming, *Nature*, 347, 339-340, 1990. doi:10.1038/347339b0
- 622 Lynch, D. K.: *Cirrus*, Oxford University Press, 2002.
- 623 Ma, X., von Salzen, K., and Li, J.: Modelling sea salt aerosol and its direct and indirect effects
624 on climate, *Atmospheric Chemistry and Physics*, 8, 1311-1327, 2008.
- 625 Maier-Reimer, E., Kriest, I., Segschneider, J., and Wetzol, P.: The Hamburg Oceanic Carbon
626 Cycle Circulation model HAMOCC5.1, Max Planck Institute for Meteorology,
627 Hamburg, Germany, 2005.
- 628 Matthews, H. D., Cao, L., and Caldeira, K.: Sensitivity of ocean acidification to
629 geoengineered climate stabilization, *Geophysical Research Letters*, 36, 2009.
630 doi:10.1029/2009gl037488
- 631 Mitchell, D., L. and Finnegan, W.: Modification of cirrus clouds to reduce global warming,
632 *Environmental Research Letters*, 4, 045102, 2009. doi:10.1088/1748-9326/4/4/045102
- 633 Muri, H., Kristjansson, J. E., Storelvmo, T., and Pfeffer, M. A.: The climatic effects of
634 modifying cirrus clouds in a climate engineering framework, *J. Geophys. Res.-Atmos.*,
635 119, 4174-4191, 2014. doi:10.1002/2013jd021063
- 636 Niemeier, U., Schmidt, H., Alterskjaer, K., and Kristjansson, J. E.: Solar irradiance reduction
637 via climate engineering: Impact of different techniques on the energy balance and the
638 hydrological cycle, *J. Geophys. Res.-Atmos.*, 118, 11905-11917, 2013.
639 doi:10.1002/2013jd020445
- 640 Partanen, A.-I., Keller, D. P., Korhonen, H., and Matthews, H. D.: Impacts of sea spray
641 geoengineering on ocean biogeochemistry, *Geophysical Research Letters*, 43, 7600-
642 7608, 2016. doi:10.1002/2016gl070111
- 643 Riahi, K., Rao, S., Krey, V., Cho, C. H., Chirkov, V., Fischer, G., Kindermann, G.,
644 Nakicenovic, N., and Rafaj, P.: RCP 8.5-A scenario of comparatively high greenhouse
645 gas emissions, *Climatic Change*, 109, 33-57, 2011. doi:10.1007/s10584-011-0149-y
- 646 Six, K. D. and Maier-Reimer, E.: Effects of plankton dynamics on seasonal carbon fluxes in
647 an ocean general circulation model, *Global Biogeochemical Cycles*, 10, 559-583,
648 1996. doi:10.1029/96gb02561



- 649 Storelvmo, T., Kristjansson, J. E., Muri, H., Pfeffer, M., Barahona, D., and Nenes, A.: Cirrus
650 cloud seeding has potential to cool climate, *Geophysical Research Letters*, 40, 178-
651 182, 2013. doi:10.1029/2012gl054201
- 652 Teller, Edward, Roderick Hyde, Muriel Ishikawa, et al. *Active Stabilization of Climate:
653 Inexpensive, Lowrisk, near-Term Options for Preventing Global Warming and Ice
654 Ages Via Technologically Varied Solar Radiative Forcing*. Lawrence Livermore
655 National Library, 30 November. 2003
- 656 Thomson, A. M., Calvin, K. V., Smith, S. J., Kyle, G. P., Volke, A., Patel, P., Delgado-Arias,
657 S., Bond-Lamberty, B., Wise, M. A., Clarke, L. E., and Edmonds, J. A.: RCP4.5: a
658 pathway for stabilization of radiative forcing by 2100, *Climatic Change*, 109, 77-94,
659 2011. doi:10.1007/s10584-011-0151-4
- 660 Tilmes, S., Mills, M. J., Niemeier, U., Schmidt, H., Robock, A., Kravitz, B., Lamarque, J. F.,
661 Pitari, G., and English, J. M.: A new Geoengineering Model Intercomparison Project
662 (GeoMIP) experiment designed for climate and chemistry models, *Geoscientific
663 Model Development*, 8, 43-49, 2015. doi:10.5194/gmd-8-43-2015
- 664 Tjiputra, J. F., Grini, A., and Lee, H.: Impact of idealized future stratospheric aerosol
665 injection on the large scale ocean and land carbon cycles, *Journal of Geophysical
666 Research: Biogeosciences*, 120, doi: 10.1002/2015jg003045, 2016.
667 doi:10.1002/2015jg003045
- 668 Tjiputra, J. F., Roelandt, C., Bentsen, M., Lawrence, D. M., Lorentzen, T., Schwinger, J.,
669 Seland, O., and Heinze, C.: Evaluation of the carbon cycle components in the
670 Norwegian Earth System Model (NorESM), *Geoscientific Model Development*, 6,
671 301-325, 2013. doi:10.5194/gmd-6-301-2013
- 672 Wanninkhof, R.: Relationship between wind speed and gas exchange over the ocean, *Journal
673 of Geophysical Research*, 97, 7373-7382, 1992.
- 674 Weisenstein, D. K., Keith, D. W., and Dykema, J. A.: Solar geoengineering using solid
675 aerosol in the stratosphere, *Atmospheric Chemistry and Physics*, 15, 11835-11859,
676 2015. doi:10.5194/acp-15-11835-2015
- 677 Wigley, T.M.L., A combined mitigation/geoengineering approach to climate stabilization,
678 *Science* 314:452-454. 2006. doi:10.1126/science.1131728
- 679 Xia, L., Robock, A., Tilmes, S., and Neely III, R. R.: Stratospheric sulfate geoengineering
680 could enhance the terrestrial photosynthesis rate, *Atmospheric Chemistry and Physics*,
681 16, 1479-1489, 2016. doi:10.5194/acp-16-1479-2016
- 682 Zeller, D., Palomares, M. L. D., Tavakolie, A., Ang, M., Belhabib, D., Cheung, W. W. L.,
683 Lam, V. W. Y., Sy, E., Tsui, G., Zylich, K., and Pauly, D.: Still catching attention: Sea
684 Around Us reconstructed global catch data, their spatial expression and public
685 accessibility, *Marine Policy*, 70, 145-152, 2016. doi:10.1016/j.marpol.2016.04.046
686

687 FIGURES AND TABLES

688 **Figure 1. Time series of global average change in (a) oxygen content at 200-600m depth (%) and (b) SST (°C).**
689 **The oxygen change is relative to the 1971-2000 average in the historical run.**

690



691 Figure 2. The absolute change in oxygen concentration (200-600m) in 2071-2100 relative to 1971-2000 (in
692 moles O₂ m⁻²). Panel (a) shows zonally averaged (in 2° latitude bands) change for all simulations. Global maps
693 of (b) RCP8.5, (c) RCP4.5, (d) RCP8.5 with SAI, (e) RCP8.5 with MSB, (f) RCP8.5 with CCT. Gray shading in b)-f)
694 indicates areas where the change is not significantly different from the 1971-2000 average (*i.e.* within one
695 standard deviation).

696
697 Figure 3. The absolute change in sea surface temperature (SST) in 2071-2100 relative to 1971-2000 (in °C).
698 Panel (a) shows zonally averaged (in 2° latitude bands) change for all simulations. Global maps of (b) RCP8.5,
699 (c) RCP4.5, (d) RCP8.5 with SAI, (e) RCP8.5 with MSB, (f) RCP8.5 with CCT. Gray shading in b)-f) indicates
700 areas where the change is not significantly different from the 1971-2000 average (*i.e.* within one standard
701 deviation).

702
703 Figure 4. Time series of global average change in (a) atmospheric CO₂ (ppm), (b) air-sea CO₂ flux (PgC yr⁻¹), (c)
704 global surface ocean pH, (d) global deep ocean (>2000 m) pH, and (e) deep (>2000 m) North Atlantic Ocean
705 (north of 30°N) pH.

706
707 Figure 5. Time series of changes global ocean primary production (PP, %). The primary production change is
708 relative to the 1971-2000 average in the historical run.

709
710 Figure 6. The percent changes in primary production in 2071-2100 relative to the 1971-2000 average in the
711 historical run. (a) zonally averaged (in 2° latitude bands) change for all simulations. (b) RCP8.5, (c) RCP4.5, (d)
712 RCP8.5 with SAI, (e) RCP8.5 with MSB, (f) RCP8.5 with CCT. Gray shading in b)-f) indicates areas where the
713 change is not significantly different from the 1971-2000 average (*i.e.* within one standard deviation). The
714 outlined areas in panel (b) indicate regions plotted in Figure 8.

715
716 Figure 7. Time series of the 5-year running mean of globally averaged primary production (PP, %) calculated
717 offline using Equation 1, plotted as the percent change relative to the 1971-2000 average in the historical
718 run. Note the different scales on the y-axes. See Table 1 for an explanation of the different calculations
719 shown.

720
721 Figure 8. Offline calculated primary production change (PP, %) in five different regions (as indicated on Figure
722 6b) for RCP4.5, RCP8.5, and RCP8.5 with three different RM methods.

723
724 Table 1. Description of the offline calculations of ocean primary production and its primary drivers using
725 Equation 1. T is temperature, L is shortwave radiation at the surface, N is the concentration of the limiting
726 nutrient (either nitrate, phosphate, silicate, or dissolved iron), and P is the concentration of phytoplankton
727 cells. \bar{X} denotes the long-term (80 year) mean of the given variable.

Calculation	
Everything changes	T, L, N, P
Only temperature changes	T, \bar{L} , \bar{N} , \bar{P}
Only shortwave radiation changes	L, \bar{T} , \bar{N} , \bar{P}
Only phytoplankton concentration changes	P, \bar{L} , \bar{N} , \bar{T}

728

729 Table 2. General description of model experiments used in this study.

Experiment	Description	Time period
RCP4.5	Reference RCP4.5 scenario	2006-2100
RCP8.5	Reference RCP8.5 scenario	2006-2150
SAI	RCP8.5 scenario where sulfur particles are injected into the atmosphere to scatter incoming shortwave radiation and bring down global average temperatures	2020-2100
SAI _{EXT}	The extension of the SAI run after termination of climate engineering in 2100	2101-2150
MSB	RCP8.5 scenario where salt particles are added to the marine boundary layer between 45°S and 45°N to make both the sky and clouds brighter, thus increasing	2020-2100



	the Earth's albedo thereby lower global average temperatures	
MSB _{EXT}	The extension of the MSB run after termination of climate engineering in 2100	2101-2150
CCT	RCP8.5 scenario where cirrus clouds are thinned out. Cirrus clouds have a net heating effect so thinner clouds will result in lower global average temperatures	2020-2100
CCT _{EXT}	The extension of the CCT run after termination of climate engineering in 2100	2101-2150

730

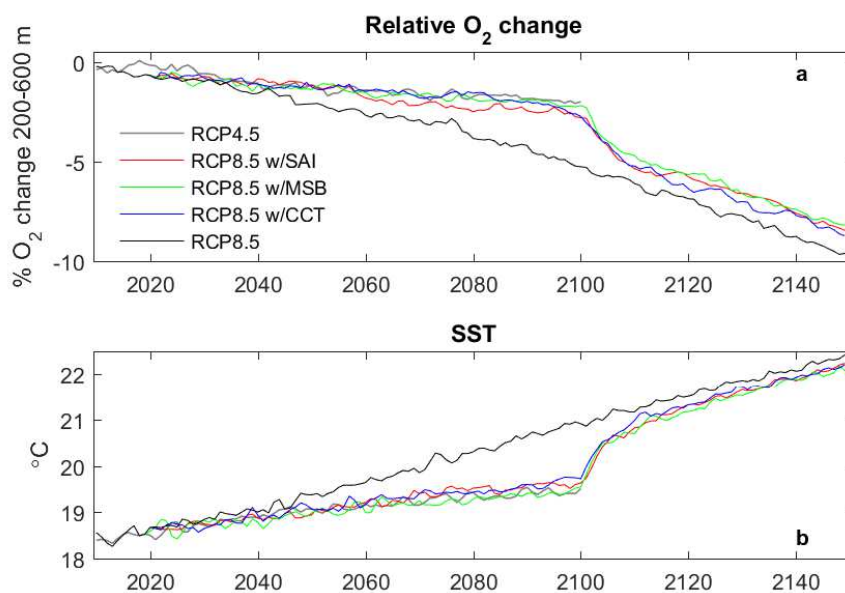


Figure 1. Time series of global average change in (a) oxygen content at 200-600m depth (%) and (b) SST (°C). The oxygen change is relative to the 1971-2000 average in the historical run.

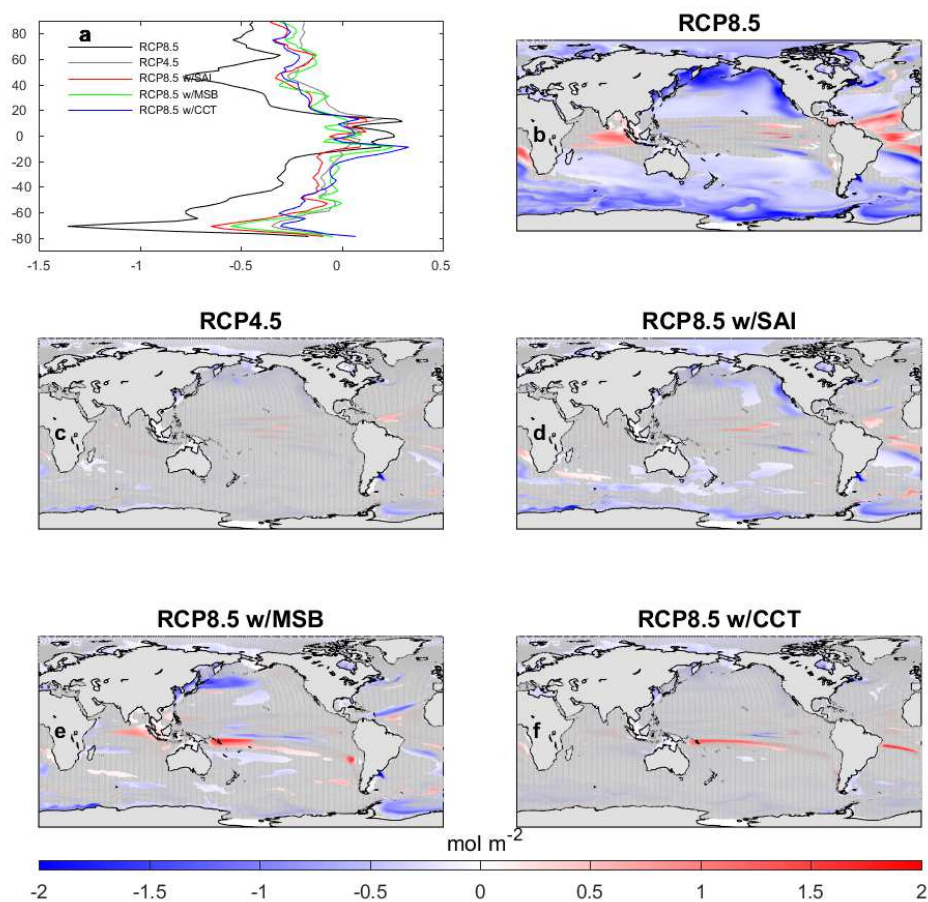


Figure 2. The absolute change in oxygen concentration (200-600m) in 2071-2100 relative to 1971-2000 (in moles $O_2 m^{-2}$). Panel (a) shows zonally averaged (in 2° latitude bands) change for all simulations. Global maps of (b) RCP8.5, (c) RCP4.5, (d) RCP8.5 with SAI, (e) RCP8.5 with MSB, (f) RCP8.5 with CCT. Gray shading in b)-f) indicates areas where the change is not significantly different from the 1971-2000 average (*i.e.* within one standard deviation).

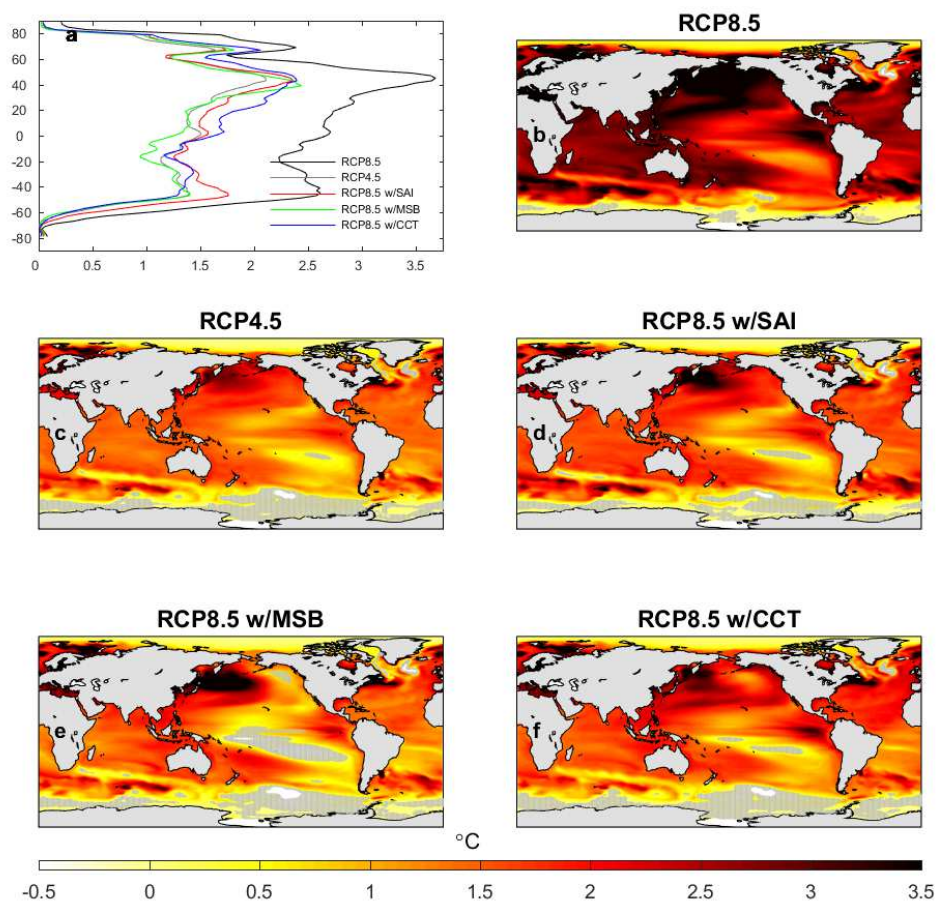


Figure 3. The absolute change in sea surface temperature (SST) in 2071-2100 relative to 1971-2000 (in °C). Panel (a) shows zonally averaged (in 2° latitude bands) change for all simulations. Global maps of (b) RCP8.5, (c) RCP4.5, (d) RCP8.5 with SAI, (e) RCP8.5 with MSB, (f) RCP8.5 with CCT. Gray shading in b)-f) indicates areas where the change is not significantly different from the 1971-2000 average (*i.e.* within one standard deviation).

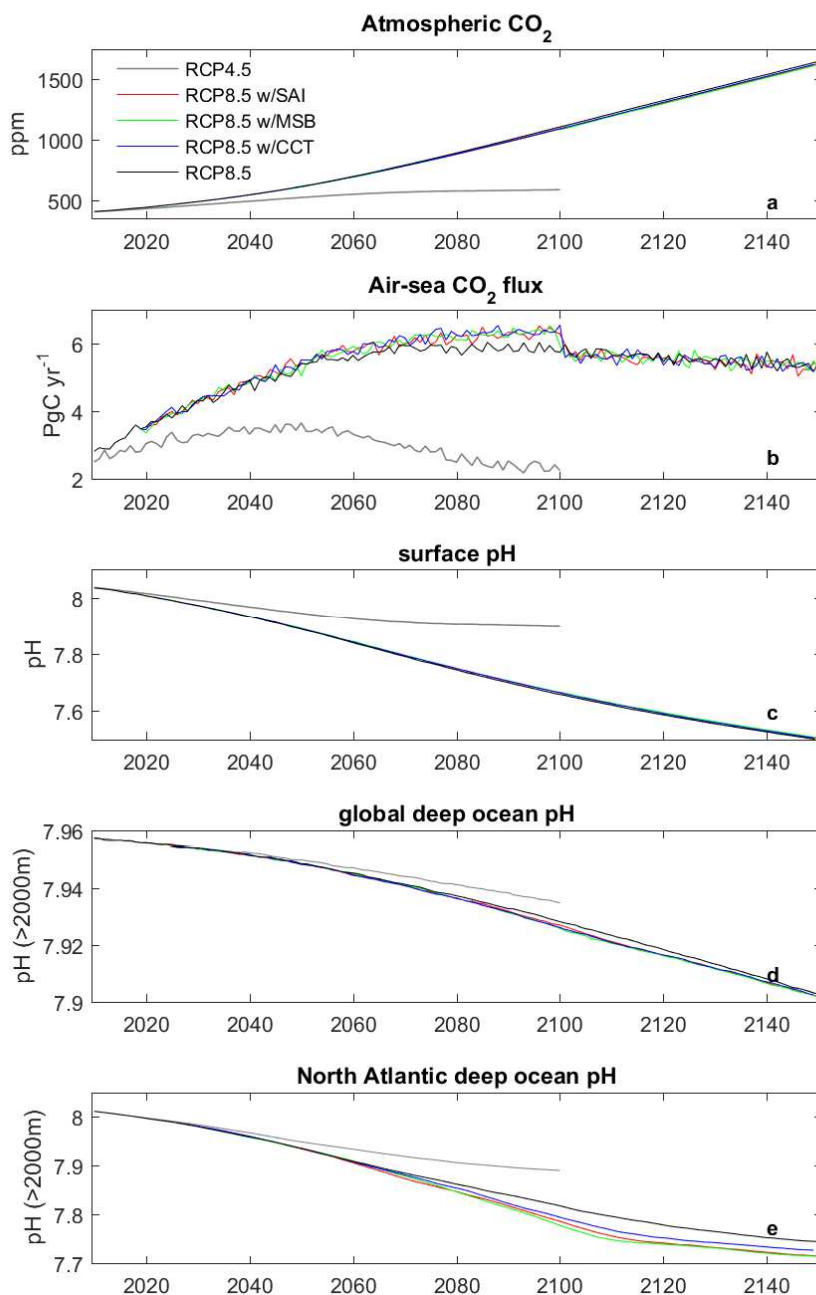


Figure 4. Time series of global average change in (a) atmospheric CO₂ (ppm), (b) air-sea CO₂ flux (PgC yr⁻¹), (c) global surface ocean pH, (d) global deep ocean (>2000 m) pH, and (e) deep (>2000 m) North Atlantic Ocean (north of 30°N) pH.

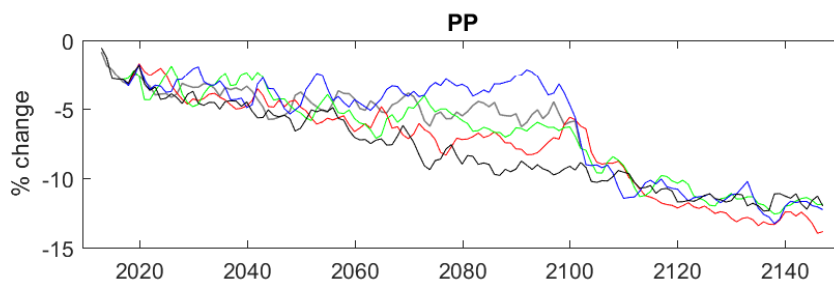


Figure 5. Time series of changes global ocean primary production (PP, %). The primary production change is relative to the 1971-2000 average in the historical run.

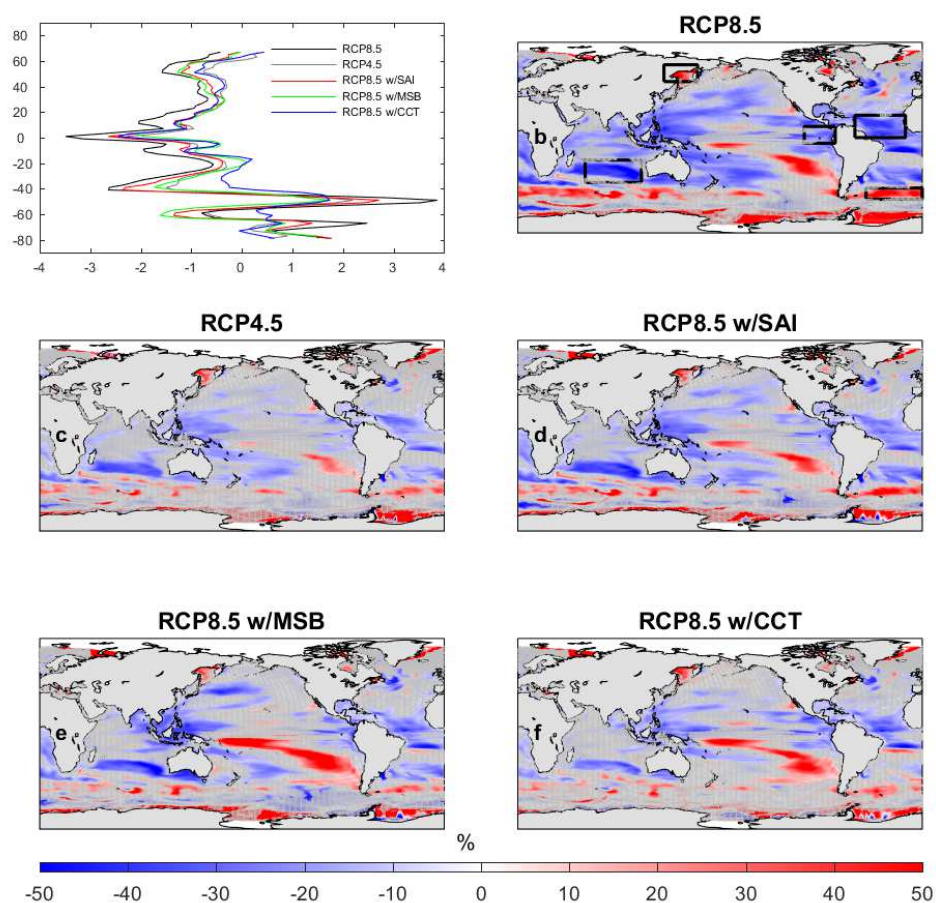


Figure 6. The percent changes in primary production in 2071-2100 relative to the 1971-2000 average in the historical run. (a) zonally averaged (in 2° latitude bands) change for all simulations. (b) RCP8.5, (c) RCP4.5, (d) RCP8.5 with SAI, (e) RCP8.5 with MSB, (f) RCP8.5 with CCT. Gray shading in b)-f) indicates areas where the change is not significantly different from the 1971-2000 average (*i.e.* within one standard deviation). The outlined areas in panel (b) indicate regions plotted in Figure 8.

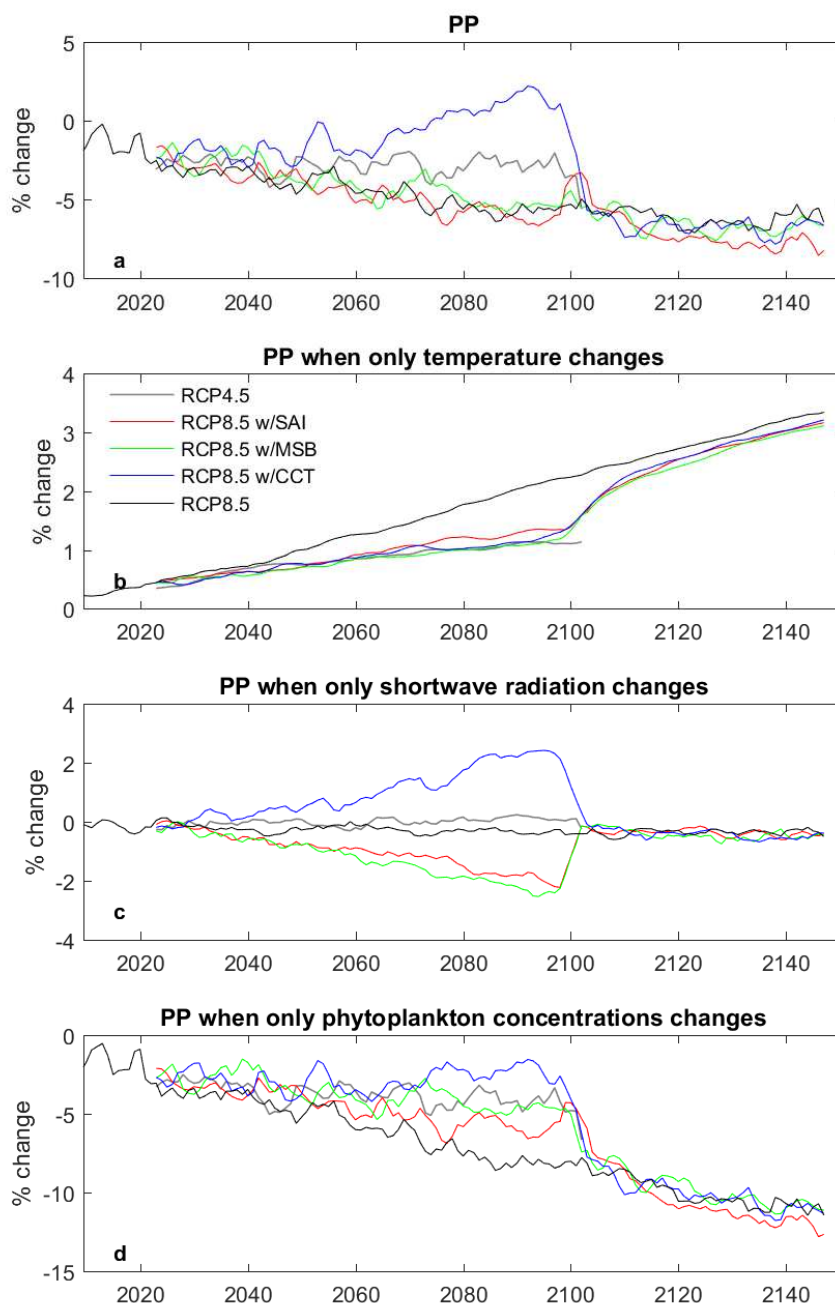


Figure 7. Time series of the 5-year running mean of globally averaged primary production (PP, %) calculated offline using Equation 1, plotted as the percent change relative to the 1971-2000 average in the historical run. Note the different scales on the y-axes. See Table 1 for an explanation of the different calculations shown.

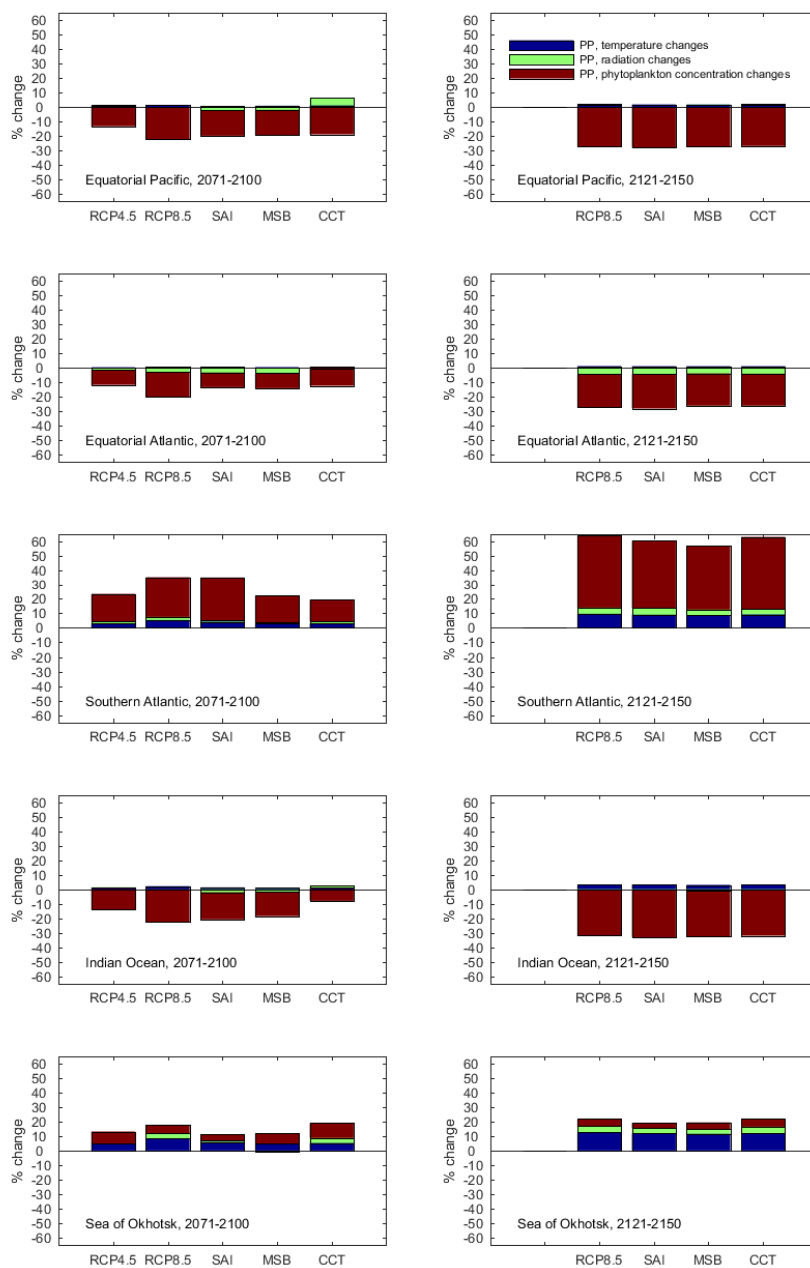


Figure 8. Offline calculated primary production change (PP, %) in five different regions (as indicated on Figure 6b) for RCP4.5, RCP8.5, and RCP8.5 with three different RM methods.